

Enhanced bone regeneration of the silk fibroin electrospun scaffolds through the modification of the graphene oxide functionalized by BMP-2 peptide

This article was published in the following Dove Medical Press journal:
International Journal of Nanomedicine

Jiannan Wu^{1,2,*}
Ao Zheng^{1,2,*}
Yang Liu³
Delong Jiao^{1,2}
Deliang Zeng^{1,2}
Xiao Wang^{1,2}
Lingyan Cao^{1,2}
Xinquan Jiang^{1,2}

¹Department of Prosthodontics, Oral Bioengineering and Regenerative Medicine Lab, Shanghai Key Laboratory of Stomatology, Ninth People's Hospital Affiliated to Shanghai JiaoTong University, School of Medicine, Shanghai 200011, China;

²Shanghai Engineering Research Center of Advanced Dental Technology and Materials, Shanghai 200011, China; ³The State Key Laboratory of Bioreactor Engineering, East China University of Science and Technology, Shanghai 200237, China

*These authors contributed equally to this work

Correspondence: Xinquan Jiang; Lingyan Cao
Department of Prosthodontics, Oral Bioengineering and Regenerative Medicine Lab, Shanghai Key Laboratory of Stomatology, Ninth People's Hospital Affiliated to Shanghai JiaoTong University, School of Medicine, 639 Zhizaoju Road, Shanghai 200011, China
Tel +86 21 6313 5412
Fax +86 21 6313 6856
Email linya.lingyancao@gmail.com; xinquanj@aliyun.com

Introduction: Bone tissue engineering has become one of the most effective methods to treat bone defects. Silk fibroin (SF) is a natural protein with no physiological activities, which has features such as good biocompatibility and easy processing and causes minimal inflammatory reactions in the body. Scaffolds prepared by electrospinning SF can be used in bone tissue regeneration and repair. Graphene oxide (GO) is rich in functional groups, has good biocompatibility, and promotes osteogenic differentiation of stem cells, while bone morphogenetic protein-2 (BMP-2) polypeptide has an advantage in promoting osteogenesis induction. In this study, we attempted to graft BMP-2 polypeptide onto GO and then bonded the functionalized GO onto SF electrospun scaffolds through electrostatic interactions. The main purpose of this study was to further improve the biocompatibility of SF electrospun scaffolds, which could promote the osteogenic differentiation of bone marrow mesenchymal stem cells and the repair of bone tissue defects.

Materials and methods: The successful synthesis of GO and functionalized GO was confirmed by transmission electron microscope, X-ray photoelectron spectroscopy, and thermogravimetric analysis. Scanning electron microscopy, atomic force microscopy, mechanical test, and degradation experiment confirmed the preparation of SF electrospun scaffolds and the immobilization of GO on the fibers. In vitro experiment was used to verify the biocompatibility of the composite scaffolds, and in vivo experiment was used to prove the repairing ability of the composite scaffolds for bone defects.

Results: We successfully fabricated the composite scaffolds, which enhanced biocompatibility, not only promoting cell adhesion and proliferation but also greatly enhancing in vitro osteogenic differentiation of bone marrow stromal cells using either an osteogenic or non-osteogenic medium. Furthermore, transplantation of the composite scaffolds significantly promoted in vivo bone formation in critical-sized calvarial bone defects.

Conclusion: These findings suggested that the incorporation of BMP-2 polypeptide-functionalized GO into chitosan-coated SF electrospun scaffolds was a viable strategy for fabricating excellent scaffolds that enhance the regeneration of bone defects.

Keywords: bone morphogenetic protein-2, peptide, osteogenic differentiation, bone regeneration, graphene oxide, silk fibroin, electrospinning scaffold, bone marrow mesenchymal stem cells

Introduction

Tissue-engineered scaffolds have biological functions, which can be applied to the regeneration and repair of bone tissue defects.¹⁻³ A good biological scaffold should

have an appropriate degradation rate and biocompatibility, as well as the ability to simulate the inner environment of cells in the body to the largest extent.⁴⁻⁶ Electrospun scaffolds have a distinctive microstructure and can simulate the reticular structure of extracellular matrix, which contributes to cell adhesion and the infiltration of nutrients to create a good microenvironment for cell migration, proliferation, and differentiation.^{7,8}

Silk fibroin (SF) is a natural high-molecular material. SF is rich in hydrophilic amino acid side chains, which improves its hydrophilicity and biocompatibility.⁹ Besides, its degradation products can be fully absorbed by the body.¹⁰ In recent years, SF electrospun scaffolds have been broadly studied in the field of tissue defect regeneration.^{11,12} Bhattacharjee et al mixed hydroxyapatite with SF to produce an electrospun scaffold; bone marrow mesenchymal stem cells (BMSCs) were seeded on the scaffold and implanted into the body. It was found that these scaffolds could well repair bone defects, suggesting that SF was an excellent scaffold material for bone tissue engineering.¹³ However, SF has poor osteoinduction, which limits its application. Moreover, it needs the help of other active factors to exert osteogenesis.¹⁴ This inspired us to find a suitable way to modify SF scaffolds with active factors to promote bone regeneration. Chitosan (CS) is a natural alkaline polysaccharide with an excellent biocompatibility. It can be compounded with active factors to guide the repair of bone tissue defects.¹⁵ Most importantly, it can interact with a large number of water-soluble anionic polymers (eg, sodium alginate, glycoprotein, and other negative bioactive substances) to form polyelectrolyte complexes because of its special positively charged and high charge density. Accordingly, CS coatings can make the scaffolds electropositive.¹⁶

Graphene oxide (GO) is a derivative of graphene with a typical quasi-two-dimensional (2D) spatial structure.¹⁷ The GO has high specific surface energy, good hydrophilicity and mechanical properties, and good dispersion stability in water and most polar organic solvents.¹⁸ It can be connected with other functional groups or materials through covalent bonds as it contains a large number of reactive oxygen-containing functional groups, such as epoxy groups, hydroxyl groups, and carboxylic acid groups.^{19,20} Many studies have shown that combining GO with active factors or drugs not only endows the drugs with targeted and controlled properties, presenting better therapeutic effects, but also improves its biocompatibility.²¹⁻²³ When implanted into the body, the scaffolds containing GO can be degraded by the secretion of peroxidase from immune cells and finally be excreted through urine and feces.²⁴⁻²⁶ Besides, GO has π - π stacking, electrostatic, and

hydrogen bonding interactions. It also has enriching effects on various active factors in body fluids.²⁷ Moreover, the negative charge of GO helps to combine it with positively charged macromolecules.²⁸ The above characteristics make GO suitable for being used as a new carrier material.

Bone morphogenetic protein-2 (BMP-2) has been found to be critical for osteogenesis and bone metabolism.²⁹⁻³¹ However, the preparation process of BMP-2 is complex and the production rate is low.^{32,33} In addition, large dose applications may produce side effects, eg, edema, heterotopic bone formations, and immunological reactions.³⁴⁻³⁶ Many studies have reported a new 24-amino acid polypeptide known as P24 (S^(PO4)KIPKASSVPTELSAISTLYLDDD). The polypeptide originates from the knuckle epitope of BMP-2 with a similar osteogenic activity to BMP-2.³⁷ It not only increases BMSCs' osteoblast differentiation but also has a simple synthesis procedure, which is likely to be more practical and cheaper than using recombinant proteins.³⁸⁻⁴⁰ However, the half-life of BMP-2 polypeptide is short, and they are easy to deactivate when applied in vivo alone.⁴¹ Therefore, it is necessary to combine them with appropriate carrier materials to reduce the short half-life and facilitate rapid diffusion to improve their biological activity.

In this study, the GO surface was modified by grafting on BMP-2 polypeptide (GO-P24). Subsequently, the negatively functionalized GO was assembled on a positively CS-coated SF electrospun scaffolds through electrostatic interactions. The GO functionalized with BMP-2 polypeptide was immobilized on the electrospun scaffolds to further improve the biocompatibility of the scaffolds, which not only promoted cell adhesion, proliferation, and differentiation but also improved the osteogenesis and mineralization of BMSCs. Finally, composite scaffolds were used to transplant a critical cranial defect rat model, and the bone regeneration in the defect was evaluated by microscopic computed tomography (micro-CT). This study further showed the cooperative effects of GO and BMP-2 polypeptide in promoting osteogenesis and the potential of SF electrospun scaffolds modified by GO-P24 for applications of the engineering of bone tissue.

Materials and methods

Preparation of GO

In line with previous reports, the modified hummer method was used to synthesize GO.⁴² In brief, 100 mL of 98% H₂SO₄ was introduced to a mixture with 2 g NaNO₃ and 2 g graphite powder. It was then strongly stirred in an ice bath for 30 minutes. Next, 4 g KMnO₄ was introduced to the mixture and stirred continuously for 1 hour, after which it

was returned to ambient temperature and stirred overnight. Deionized water (600 mL) was then added to the suspension, slowly, while stirring constantly for 30 minutes. Next, 10 mL of 30% H₂O₂ was added to obtain a bright yellow–orange suspension. The suspension was centrifuged, and the precipitate was washed with 10% HCl and distilled water. The cleaned precipitate was dispersed in deionized water and then separated by ultrasound to form a single layer of GO, followed by freeze-drying to obtain pure graphite oxide. The GO was further sterilized with 10 kGy γ radiation exposure before the subsequent experiment.

Preparation of GO–P24

Nearly 4 mL GO (0.5 mg/mL) was dissolved in morpholine ethylsulfonic acid buffer (0.1 M, pH=5.6) and sonicated for 5 minutes. Subsequently, to activate the chemical bonds on the GO, 7.5 mg *N*-hydroxysuccinimide (NHS) and 5 mg 1-(3-dimethylaminopropyl)-3-ethylcarbodiimide hydrochloride (EDC) were added. After the reaction, the suspension was further incubated for 2 more hours, with the addition of 400 μ L BMP-2 polypeptide solution (2.5 mg/mL). Stirring was continued for 24 hours, and then, the reactant mixture (molecular weight [MW]: 1,000) was dialyzed against deionized water. Finally, GO–P24 conjugates were obtained by lyophilization. All solutions were filtered with sterile filter before use and ensured sterility during operation.

Electrospun scaffold fabrication

Bombyx mori cocoons were cut up for boiling in 5 g/L NaHCO₃ solution for 30 minutes and in distilled water for another 30 minutes. The above steps were repeated three times. The degummed SF was dissolved in CaCl₂/C₂H₅OH/H₂O solution (molar ratio 1:2:8) at 70°C for 4 hours and then dialyzed in deionized water for 3 days. SF was produced after lyophilization. For the SF electrospun scaffold fabrication, the SF was dissolved in hexafluoroisopropanol for a final concentration of 30% and the prepared solution was put into a syringe with a steel needle. The needle was 18 cm away from the foil receiver. The conditions for electrospinning were as follows: flow rate 0.9 mL/h and voltage 35 kV. The prepared electrospun scaffold was placed into a fume hood for later use. The scaffolds were further sterilized with 10 kGy γ radiation exposure before in vitro and in vivo experiments.

GO–P24 immobilization on the scaffold

By dissolving CS powder into 0.5% (v/v) acetic acid solution, this study prepared a 1 mg/mL CS solution. The SF scaffolds were first put into the CS solution for 20 minutes to form

CS-coated SF scaffolds. For the removal of unassembled CS, the scaffolds were then washed three times with 0.1 mg/mL NaCl solution. To immobilize the GO–P24 on the CS-coated SF scaffold surfaces, the scaffolds were immersed in the dispersion of GO–P24 for 6 hours while shaking. Next, the prepared scaffolds were washed with sterile water and dried in the air for subsequent experiments.

X-ray photoelectron spectroscopy (XPS)

The modified GO's surface chemistry was studied by XPS (Escalab 250; Thermo Fisher Scientific, Waltham, MA, USA). The survey spectrum was recorded from 1,300 to 0 eV. Besides, the binding energies were calibrated in comparison to the hydrocarbon C 1 seconds peak (284.6 eV).

Fourier transform infrared spectroscopy (FTIR)

The modified GO's FTIR spectra were measured with an FTIR spectrophotometer (Nicolet 5DXC spectrometer; Thermo Fisher Scientific, Waltham, MA, USA) using the KBr pellet (10 mm in diameter) method. The 2 mg GO or GO–P24 was mixed with 100 mg KBr in mortar and pressed to prepare pellets for analysis. The spectra were examined within the wave range of 3,000–500 cm⁻¹.

Atomic force microscopy (AFM)

GO's surface topography and the scaffolds' surface roughness were analyzed through AFM (Multimode 8; Bruker Optik GmbH, Ettlingen, Germany). The GO was evenly dispersed on aluminum foil, and the imaging of the fibers was present in a normal atmosphere, with a silicon cantilever probe. To measure the average surface roughness, three tests were estimated at different locations.

Transmission electron microscope (TEM) and scanning electron microscopy (SEM)

With the use of SEM (Hitachi-S3400N; Hitachi Ltd., Tokyo, Japan), this study observed the microstructure of the scaffolds. The scaffolds were fixed on the stub and covered with gold. The microstructure was observed at an accelerating voltage of 10 kV. Moreover, the GO was assessed by a TEM (JME-100CX; JEOL, Tokyo, Japan).

Zeta potential

With the use of a laser particle analyzer (ZETA-AIZER; Malvern Instruments, Malvern, UK) and following a dynamic light scattering, this study determined the zeta potential of SF, CS, GO, and GO–P24.

Mechanical properties of scaffolds

The scaffolds were cut into rectangular strips of $5 \times 30 \times 0.05$ mm in size. The tensile properties of the samples were investigated by an electronic universal testing machine (HY00230; Hengyi, China) coupled with 100 N force sensor. The measurement speed was 5 mm/min, and the gage length was 5 mm at 25°C and under 50% relative humidity.

Degradation experiment of scaffolds

PBS solution was applied for degradation experiment in vitro. The samples were immersed in PBS solution and extracted out every 3 days. In the meantime, the PBS solution in other samples was replaced and degraded continuously. The degradation experiment lasted for 20 days. This study washed the samples with distilled water 3 times, removing inorganic salts and vacuum drying. After the sample was accurately weighed, the degradation rate was calculated. Degradation rate (%) = $(W^a - W^b) / W^a \times 100\%$, where W^a is the mass of the scaffolds before degradation and W^b denotes the mass of the scaffolds after degradation.

Isolation and culture of cells

Rats (3 weeks old, 100–120 g) were anesthetized with 2% pentobarbital sodium to remove the femur and tibia under aseptic conditions and collect bone marrow cells. This study cultured the cells in 25 cm² cell culture flasks in DMEM supplemented with 10% FBS (Thermo Fisher Scientific, Waltham, MA, USA), and incubated in an atmosphere of 5% CO₂ at 37°C. After 2 days, the culture medium was replaced, and any unattached cells were removed. The cells between the fourth and sixth passage were used for subsequent experiments. All animals used in our experiment were approved by the Committee of Experimental Animal Administration of Shanghai Ninth People's Hospital, affiliated with Shanghai Jiao Tong University School of Medicine. Besides, all procedures followed by international ethics guidelines and the National Institutes of Health Guide concerning the Care and Use of Laboratory Animals.

Cell proliferation

The scaffolds were classified into four groups, namely the SF group (SF group), the SF-CS group (SF-CS group), the SF-CS-GO-P24 group, and the SF-CS-GO group. By using cell counting kit-8 (CCK-8) assay (CCK-8 Kit; Beyo Biotech, Shanghai, China), this study assessed cells proliferation of BMSCs seeded on the four different groups of scaffolds (diameter: 5 mm) at a density of 4×10^3 cells per well in a 96-well plate at 1, 3, 5, and 7 days. In brief, this study replaced the culture

medium with 100 μ L DMEM and 10 μ L CCK-8 solution at the relevant time point. This study incubated samples at 37°C for 1.5 hours and transferred 100 μ L of the supernatant to a clean 96-well plate. By the use of a microplate reader, this study measured the absorbance at 450 nm (Thermo LabSystems, Beverly, MA, USA). For the assay of cell viability, this study used three parallel experimental samples.

Cell adhesion

Under a confocal laser scanning microscope (TCS SP5; Leica Microsystems, Wetzlar, Germany), this study observed the adhesion of BMSCs to the different groups of scaffolds at 24 hours. In brief, this study fixed the cells cultured on the scaffolds (diameter: 5 mm) in a 96-well plate, and the cell density was 4×10^3 cells per well with 4% paraformaldehyde for 30 minutes at 37°C. Subsequently, these cells were rinsed with PBS three times. Next, these scaffolds were permeabilized with 15 minutes immersion in 0.5% PBS Triton X-100 at ambient temperature and then washed three times in the PBS. Afterward, the cells were stained with FITC-phalloidin for 1 hour at 37°C to stain the cytoskeletons. Finally, the cytoskeleton and the cell morphology were observed at 488 nm (laser intensity: 5%) using a confocal laser scanning microscope. For the assessment of the cell distribution and morphology, this study used three views.

Live/dead assay

To verify the cytotoxicity of the scaffolds, we further conducted a live/dead cytotoxicity assay. The BMSCs were cultured on the different groups of scaffolds (diameter: 5 mm) for 24 hours in a 96-well plate at a density of 1×10^4 cells per well. Next, this study washed the scaffolds with PBS for 5 minutes and incubated with 4.5 μ M propidium iodide and 2 μ M calcein acetoxymethyl for 30 minutes at 37°C. Subsequently, this study washed the scaffolds with PBS for 5 minutes and viewed using a confocal laser scanning microscope (laser intensity: 15%). The dead cells presented red fluorescence, and the active cells presented green fluorescence.

Protein loading and active release of P24

Loading efficacy of P24 on GO-P24 and SF-CS-GO-P24 was detected by thermogravimetric analysis (TGA). Thermal behaviors of GO, GO-P24, SF, and SF-CS-GO-P24 were respectively tested using the apparatus of thermogravimetric analyzer (TGA-50; Shimadzu, Kyoto, Japan) in an N₂ atmosphere with a heating rate of 10°C min⁻¹; the range of temperature measured from ambient temperature to 800°C. The in vitro release of P24 polypeptide from SF-CS-GO-P24 was

measured using a bicinchoninic acid (BCA) protein assay kit (Thermo Fisher Scientific). The SF-CS-GO-P24 was dispersed in PBS solution and shaken slowly for 21 days at 37°C. The supernatant was collected, and fresh equal volume of PBS was added at corresponding time points. The amount of P24 released from SF-CS-GO-P24 in the supernatant was measured following the manufacture's instruction of the BCA protein assay kit. The activity of the released P24 from SF-CS-GO-P24 scaffold was investigated through the ALP activity assay. The scaffolds of SF-CS-GO-P24 and SF-CS-GO were placed into the 24-well plate. The BMSCs were respectively seeded on the scaffolds (diameter: 15 mm) at a density of 4.0×10^4 cells per scaffold. The cells seeded on the well plate and cultured with the normal medium were used as the negative control, while cells cultured with the medium containing equivalent P24 to that contained in the SF-CS-GO-P24 scaffold were used as the positive control. The cells seeded on the scaffolds were cultured with the normal medium, and the ALP activity assay was carried out to observe the osteogenic differentiation of BMSCs 7 days later. The samples were washed with PBS and added with 200 μ L of cell lysis buffer. In all, 100 μ L of cell lysis was added to 100 μ L of reaction solution, incubated at 37°C for 30 minutes, and then terminated with 100 μ L of 0.5 mol/L NaOH. OD value was measured at 405 nm. With the use of BCA protein assay kit, this study measured protein concentration in cell lysis. The relative ALP activity = $OD_{405} / \text{total protein}$.

In vitro osteogenic differentiation

BMSCs were seeded on different scaffolds (diameter: 15 mm) in a 24-well plate at a density of 4.0×10^4 cells per well and cultured in an osteogenic medium containing 10 mM β -glycerol phosphate (Sigma-Aldrich Co., St Louis, MO, USA), 50 μ M ascorbic acid, 0.1 μ M dexamethasone, and high-glucose DMEM supplemented with 10% FBS to measure the osteogenic induction of the BMSCs. To examine osteogenic differentiation under normal conditions, scaffolds cultured in high-glucose DMEM containing 10% FBS (growth medium) were used. The culture medium was changed every 3 days, and the cells were cultured for 14 days.

Immunofluorescence staining

By using 4% (w/v) paraformaldehyde (Sigma-Aldrich Co.), this study fixed the cells cultured on the scaffolds for 30 minutes. Then, these cells were permeabilized at ambient temperature with 0.2% (v/v) Triton X-100 (Sigma-Aldrich) for 10 minutes. After samples were washed three times in PBS, this study blocked the samples for 1 hour in 10% bovine

serum (BioSera, Nuaille, France). Subsequently, this study incubated the cells with rabbit monoclonal anti-osteopontin (OPN) (ab8448; Abcam, Cambridge, MA, USA) and rabbit polyclonal anti-collagen type I (COL I) (ab34710; Abcam) overnight at 4°C, which are the primary antibodies and also the fluorescent dye-conjugated secondary antibodies (#A-11034, Alexa Fluor-488 goat anti-rabbit IgG and #A-11037, Alexa Fluor-594 donkey anti-rabbit IgG; Thermo Fisher Scientific) at an ambient temperature for 45 minutes. Using a confocal laser scanning microscopy (laser intensity: 488 nm 5%; 543 nm 30%), this study observed the fluorescent signals.

Real-time PCR (RT-PCR)

Following the TRIzol (Thermo Fisher Scientific) method, this study extracted the total RNA isolated from the scaffolds. RNA was reverse-transcribed to cDNA following the instructions of manufacturer (Takara, Kusatsu, Japan). The RT-PCR of the genes was performed using the SYBR Green RT-PCR Kit (Takara). β -actin served as a housekeeping gene for the normalization of data. RT-PCR was performed by Roche 480II Real-Time PCR System (Roche Diagnostics, Indianapolis, IN, USA) using QuantiNova SYBR Green PCR Kit (Qiagen NV, Venlo, the Netherlands). Following the $2^{-\Delta\Delta C_t}$ method, this study analyzed data. This study performed all experiments in triplicate. The following primers were used: ALP, forward 5'-GGGGTCAAAGCCAACACTACAA-3', reverse 5'-CTTCCCTGCTTTCTTTGCAC-3'; Runx2, forward 5'-GCCGGGAATGATGAGA ACTA-3', reverse 5'-GGACCGTCCACTGTCACTTT-3'; COL I, forward 5'-AATGGTGCTCCTGGTATTGC-3', reverse 5'-GGTTCACCACTGTTGCCTTT-3'; OPN, forward 5'-GATCGATAGTGCCGAGAAGC-3', reverse 5'-TGAAACTCGTGGCTCTGATG-3'; β -actin, forward 5'-CTAAGCCAACCGTGAAAAG-3', reverse 5'-TACATGGCTGGGGTGTGA-3'.

In vivo scaffold transplantation

Fifteen Sprague Dawley rats (male, 6-week-old, 200 g average body weight) randomly fell into five groups (three animals per group) and were used for the calvarial bone defect implantation of scaffolds. In brief, surgeries were performed under anesthesia in a sterile environment, and then, two round bone defects (diameter=5 mm) were created on both sides of the skull. The electrospun scaffolds of different groups (diameter: 5 mm) were implanted into the respective critical-sized bone defects. The whole calvarial bones samples containing the defect sites were explanted and fixed in 10% formalin at the eighth week after transplantation.

Micro-CT measurement

A micro-CT system (ICT-40; Scanco Medical, Bassersdorf, Switzerland) was used at a resolution of 18 μm in this study to assess the bone regeneration in the calvarial defects 8 weeks after surgery. 3D images were then created, and by using ImageJ (National Institutes of Health, Bethesda, MD, USA), the percentages of bone mineral density and new bone over total bone volume were analyzed.

Histological evaluation

This study completely decalcified all specimens in 15% EDTA solution. The decalcified samples were trimmed, dehydrated with gradient ethanol, and embedded in paraffin. A series of slices (5 mm thick) were cut from the center of the repair site and stained with Masson trichrome and H&E in accordance with standard protocols. Finally, the successful stained slices were sealed by the neutral gum. All histological sections were observed using a light microscope (Olympus IX 71; Olympus Corporation, Tokyo, Japan).

Statistics

Results are expressed as mean \pm SD. To assess statistical significance, this study used ANOVA. In all evaluations, $P < 0.05$ was set as the level of statistical significance.

Results and discussion

Morphology of the prepared GO and GO-P24

GO is a novel type of carbon material with excellent properties. It has been reported that GO could facilitate the attachment, proliferation, and osteogenic differentiation of BMSCs at suitable concentrations.^{43,44} In addition, some studies showed that GO could serve as a slow release carrier because of its π - π stacking, hydrogen bonding, and electrostatic interactions between proteins. It is rich in -COOH and other functional groups. These functional groups allow GO to chemically interact with active factors, thereby improving GO's properties and expanding the field of application of this material.²⁷ GO was synthesized following the previously reported method.⁴² BMP-2 polypeptide was then grafted onto the GO through chemical reactions. With EDC and NHS as intermediate media, the carboxyl group on GO and the amino group on the short peptide could produce a dehydration condensation reaction to form the product GO-P24. To analyze the lateral size characteristics, thickness, and morphology of the samples, this study used AFM and TEM. According to the TEM analysis, shown in Figure 1A, GO

could be seen as a transparent single layer, like a lid gauze layer, suggesting the high level of exfoliation. Owing to the incorporation of the P24 polypeptide, this study observed flecks and floccules to form on the GO sheet surface. In particular, the AFM images of GO in Figure 1B suggested that the height of the GO sheet was ~ 2 nm. After conjugation with P24, the thickness remains basically unchanged. Additionally, the GO sheet had a very flat surface. In contrast, the GO-P24 showed a comparatively coarse surface and was almost circular due to the P24 surrounding the GO; moreover, the diameter of GO-P24 was getting larger compared with GO.

Characterization of the prepared GO and GO-P24

To further confirm the successful graft of the BMP-2 polypeptide onto the GO, we performed related examinations. The formation of the GO-P24 was further investigated by FTIR, as shown in Figure 2A; in comparison with GO, the spectrum of the GO-P24 showed new absorption peaks at 1,622 and 1,550 cm^{-1} because of the formation of an amide bond. The new peaks at 800 and 838 cm^{-1} represented the characteristic peaks of the phenyl group of P24. Figure 2B and C shows the XPS spectra of GO and GO-P24. The C peak and O peak of GO appear respectively near the binding energy (BE) of 287.3 and 532.8 eV, while a significant N peak appeared on the spectrum of GO-P24 after grafting the polypeptide, which could be attributed to the N atoms in the amino acids of the polypeptide. In the C1s XPS spectrum in Figure 2D, three types of carbon atoms were present as follows: C=O, C-C, and C-O contributed to peak formations through three different binding energies in GO, while GO-P24 was composed of four types of carbon atoms: C=O, C-C, C-N, and C-O. Likewise, GO could only show N elements in air in the N1s XPS spectrum in Figure 2E, while GO-P24 could detect a BE of 398.9 eV corresponding to -CONH-. The abovementioned results suggested that GO nanosheets were successfully prepared and functionalized with BMP-2 polypeptide. GO can be better used in tissue regeneration and repair by modifying it, fully exploiting its good biocompatibility, and giving full play to its role as a carrier.

Characterization of electrospun scaffolds

The ideal scaffold material for bone repair requires biodegradability, good biocompatibility, bone conductivity, and osteoinductive activity.⁴⁵ SF is a natural biological protein and has been widely used in tissue engineering. However,

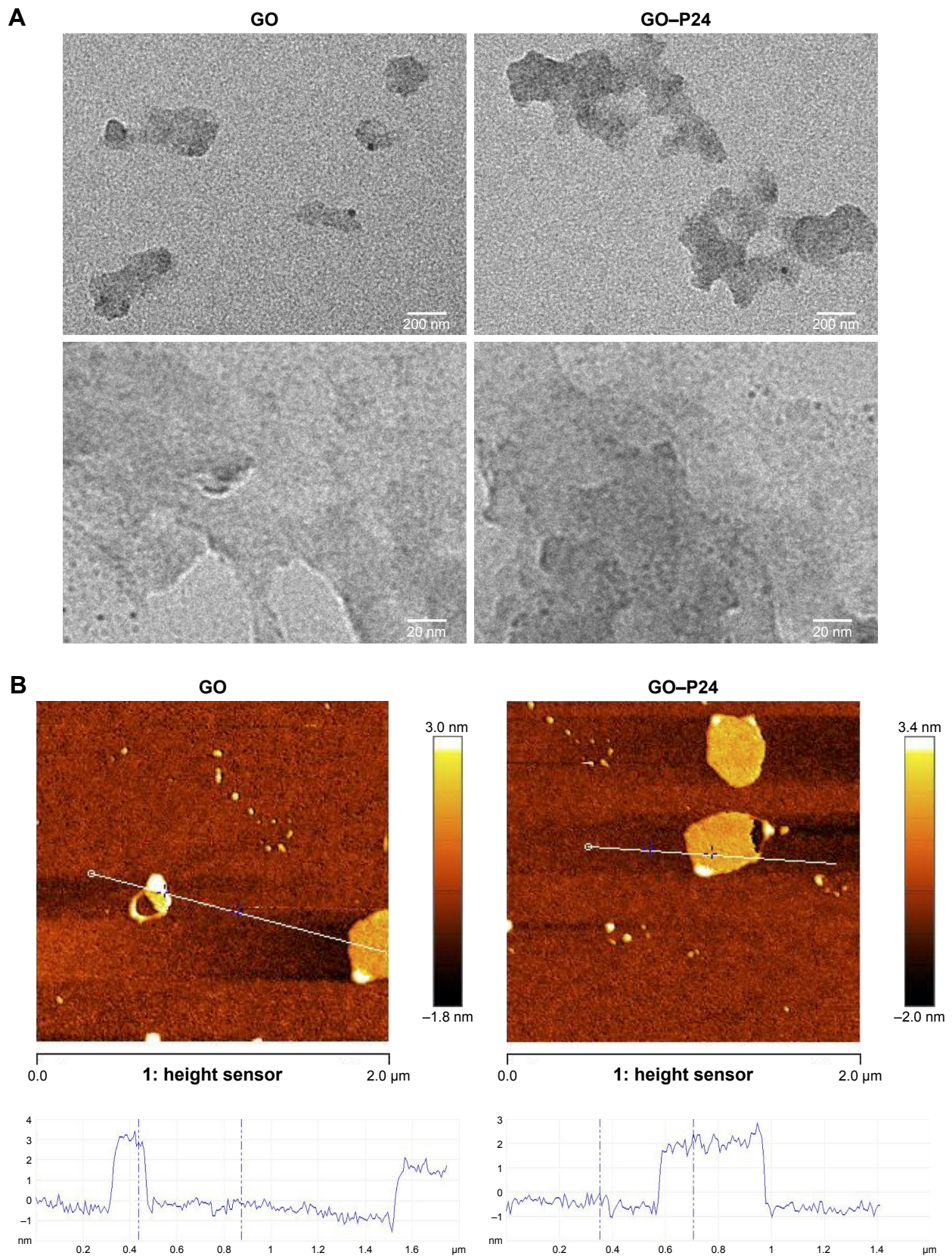


Figure 1 Morphology of GO.

Notes: (A) TEM images of GO and GO-P24. (B) Tapping mode AFM images and height profiles of GO and GO-P24.

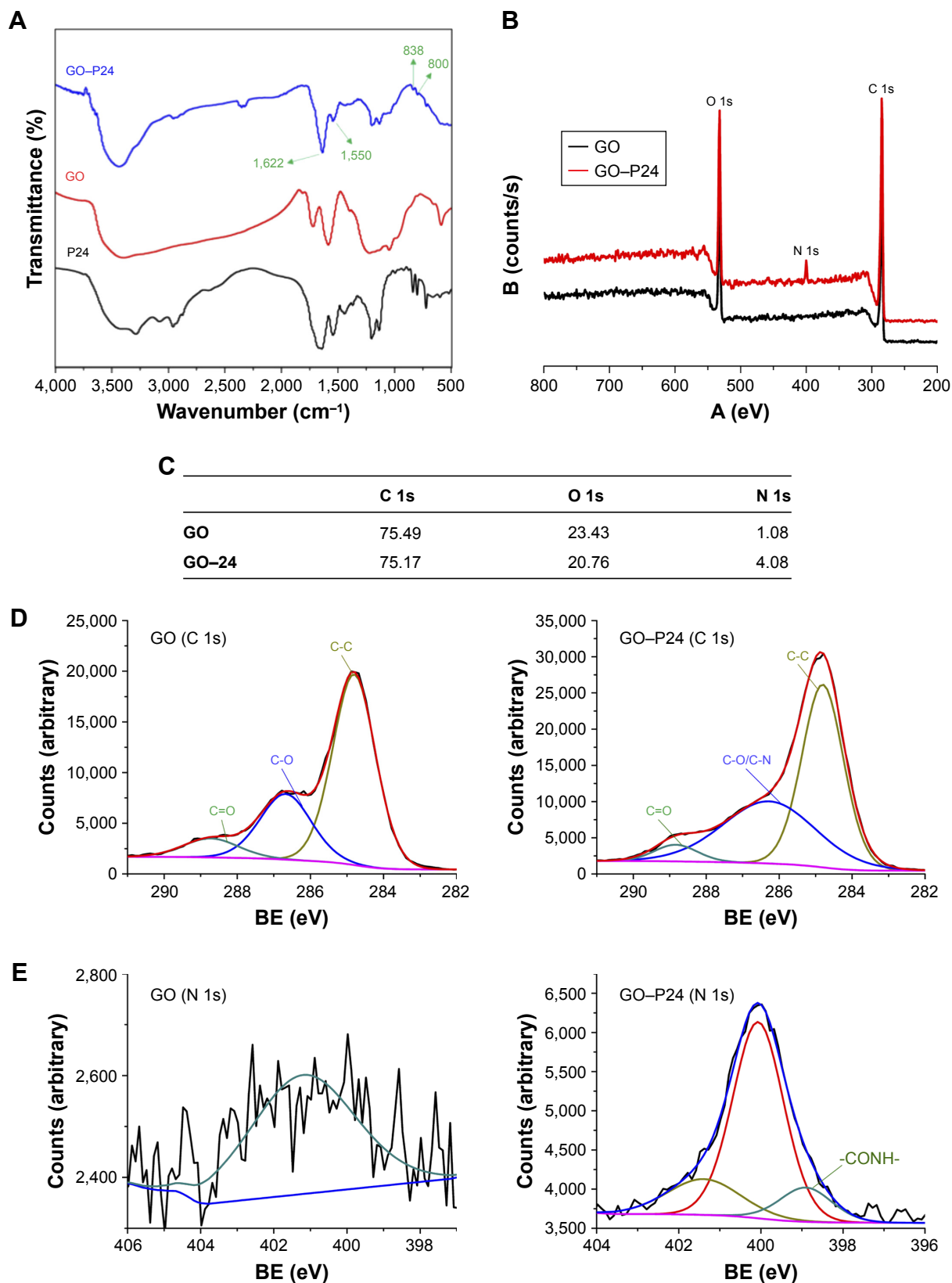


Figure 2 Surface characterization of the GO.

Notes: (A) FTIR spectrum of GO, P24, and GO-P24. (B) XPS spectrum of GO and the GO-P24. (C) Quantification of atomic chemical composition of GO and GO-P24. High-resolution XPS spectra of (D) C 1s (E) N 1s peaks of GO and GO-P24.

Abbreviations: GO, graphene oxide; FTIR, Fourier transform infrared spectroscopy; XPS, X-ray photoelectron spectroscopy; BE, binding energy.

it is usually necessary to add active factors to improve its osteogenic effects due to its weak osteoinductive activity.¹⁴ At present, the combination of biomaterials and active factors mostly adopts a simple physical adsorption method. Owing to the lack of affinity between the factors and material surface, it is easy to cause an explosive release and the active factors cannot be released continuously and stably.⁴⁶ Accordingly, the modification of SF scaffolds with GO–P24 further improved the bioactivity of the scaffolds. The average zeta potential of GO–P24 was -21.2 ± 1.2 mV, while the zeta potential of CS ranged from 15.89 ± 0.6 mV, that of the SF was -10.3 ± 0.4 mV, and that of the GO was -42.5 ± 3.2 mV. Thus, SF acted as a substrate and presented positive charge through the coating of CS, and the negatively charged GO or GO–P24 could be immobilized with the positively charged scaffolds through electrostatic interactions. The overall view images in Figure 3A suggest that CS coating on the SF scaffolds did not significantly change the color and morphology, but SF–CS–GO and SF–CS–GO–P24 show a darker color because of the unique color of GO itself. The SEM images in Figure 3B show that the contact boundaries between the fibers of the SF–CS scaffolds became blurred,

and some fibers were interconnected. The fibers boundaries of SF scaffolds, in comparison, were clear and separated from each other. The change in the microstructure might be due to the coating of CS on the surface of the scaffold fibers. Furthermore, the fibers of the SF–CS–GO and SF–CS–GO–P24 scaffolds displayed scattered nanosheets, and some of them were clustered together. These nanosheets were most likely to be GO and GO–P24 coated on the surface of the fiber through electrostatic interactions with CS. Most importantly, all of these modifications did not change the porous structure of the scaffolds. A suitable surface roughness in scaffolds contributes to cell adhesion, improving the compatibility of scaffolds and cells and actively promoting tissue regeneration. Subsequently, the surface topography of the four groups of scaffolds was tested as the AFM images shown in Figure 3C. The surfaces of the SF and SF–CS nanofibers were very smooth, whereas the surfaces of the SF–CS–GO fiber were slightly unsmooth because of the coating of the GO. The surface of the SF–CS–GO–P24 nanofibers was much rougher and more wrinkled, with some small pieces of appearance. Further investigation revealed that the GO nanosheets adhered to the surface of SF–CS nanofibers,

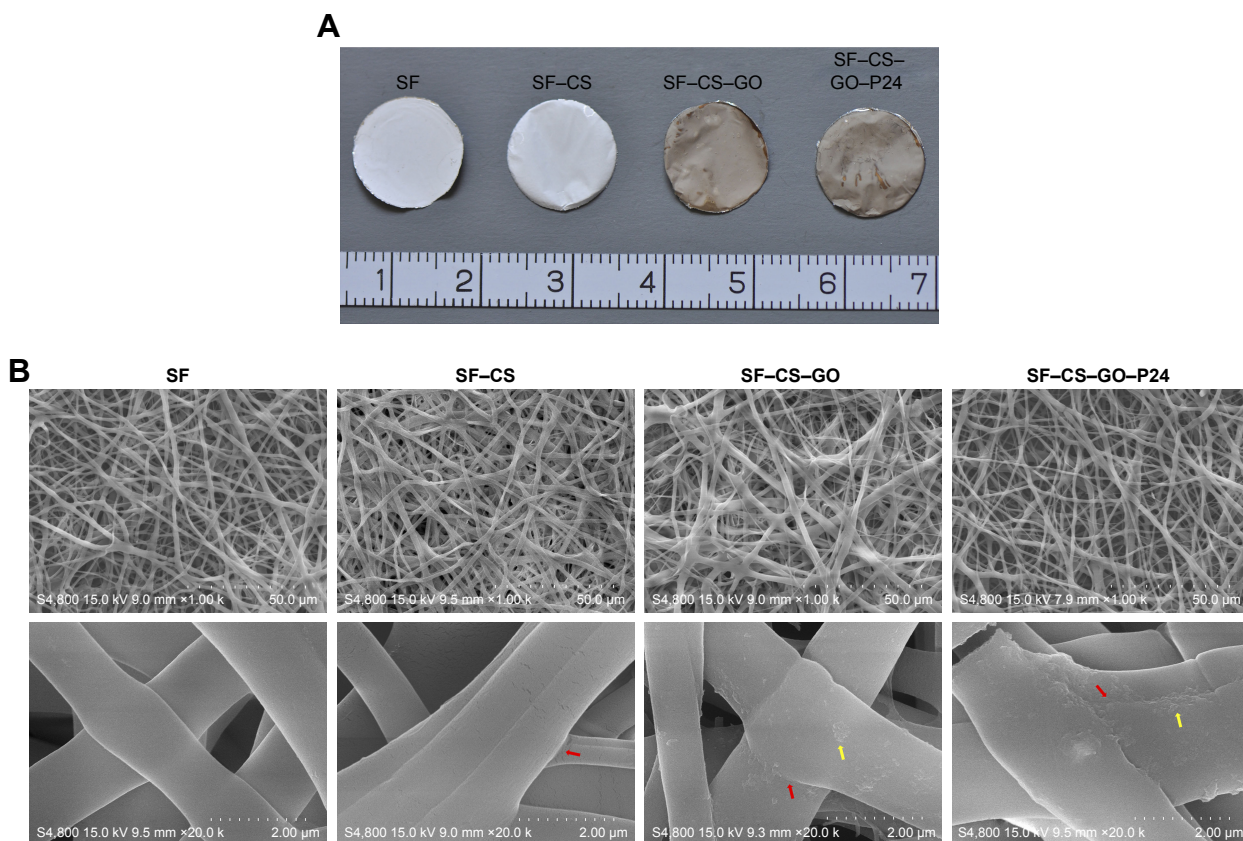


Figure 3 (Continued)

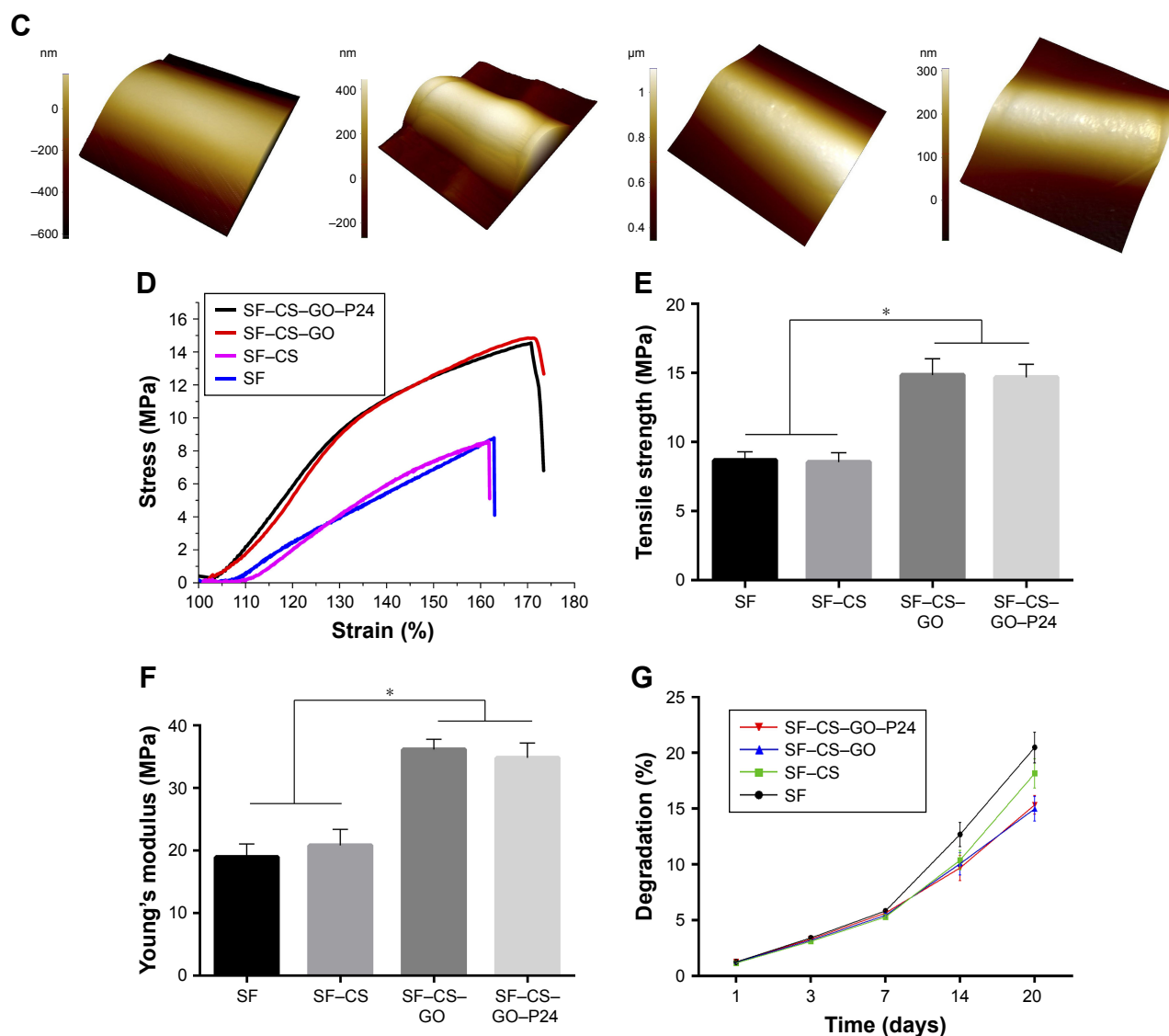


Figure 3 Characterization of electrospun scaffolds.

Notes: (A) The overall view images of the SF, SF-CS, SF-CS-GO and SF-CS-GO-P24 electrospun scaffolds. (B) SEM micrographs of four different electrospun scaffolds. The below row (scale bars=2 μm) is the magnification of the electrospun fibers to the scaffolds on the upper row (scale bars=50 μm ; red arrows: the contact boundary between the electrospun fibers; yellow arrow: the GO and GO-P24 nanosheets coated on the surface of the electrospun fibers). (C) The AFM images show the surface roughness of the four groups of the electrospun fibers. (D) Typical stress-strain curves, (E) tensile strength, and (F) Young's modulus ($n=5$, $*P<0.05$ are differences between the indicated groups). (G) In vitro degradation curve of the composite scaffolds.

Abbreviations: SF, silk fibroin; CS, chitosan; GO, graphene oxide; SEM, scanning electron microscopy; AFM, atomic force microscopy.

making the surface rougher, and this surface morphology would be conducive to cell adhesion and proliferation. The abovementioned results showed that to immobilize GO nanosheets on the surfaces of scaffolds through electrostatic interactions was simple and effective. Scaffolds used for tissue engineering should have excellent mechanical properties and a good biodegradability. Figure 3D shows the tensile stress-strain curves of electrospun scaffolds. The coating of CS had no effect on the tensile stress and the Young's modulus of SF scaffolds, but the GO or GO-P24 could improve the mechanical properties, and there was no

difference between them. This increase might be attributed to the covalent or non-covalent interactions between GO and SF.⁴⁷ In Figure 3E and F, the bare SF scaffolds held a Young's modulus of 18.84 ± 1.51 MPa and a tensile strength of 8.79 ± 0.53 MPa. For SF scaffolds modified with CS, GO, and GO-P24, the Young's modulus was 21.06 ± 2.05 MPa, 38.05 ± 1.41 MPa, and 36.17 ± 2.06 MPa, respectively, and the tensile strength was 8.58 ± 0.64 MPa, 15.34 ± 1.09 MPa, and 14.54 ± 0.84 MPa, respectively. Moreover, Figure 3G suggests that all samples exhibit similar degradation kinetics because of the porous electrospun scaffolds. The results

showed that the degradation of the four groups of scaffolds was slow and no significant difference was found in an early phase, while the degradation rate of pure SF scaffold was gradually faster than other scaffolds 2 weeks later, and the SF-CS-GO and SF-CS-GO-P24 were slower, but there was no difference between them. This might be due to the internal forces between the molecules of CS, GO, and SF, resulting in a more compact structure.⁴⁸ This was also consistent with previous reports that the transition of SF from α helical and random coils conformation to β -sheet conformation induced the intermolecular space become smaller and SF scaffolds needed to be degraded gradually under the effect of micro-environment in vivo to achieve tissue repair.⁴⁹

Biocompatibility of the composite scaffolds

To verify the cytotoxicity of the four groups of scaffolds, we first performed a live/dead assay, where live cells were labeled green and dead cells were labeled red. As shown in Figure 4A, most of the cells stayed alive after being cultured for 24 hours on the four groups of scaffolds and there were almost no dead cells in any of the groups. This result indicated that none of the scaffolds were cytotoxic, whether they were modified or not. We then observed the adhesion of cells on the scaffolds. The cell morphologies of BMSCs cultured on the different groups of scaffolds were pictured by confocal microscope after 24 hours. As shown in Figure 4B, the cells attached to all groups of scaffolds, but the morphologies were different. BMSCs adhered on the SF and SF-CS scaffolds did not spread completely and showed a round or spindle morphology. By contrast, the cells adhered on the electrospun scaffolds modified by GO, especially in the SF-CS-GO-P24 group, were fully spread, the cytoskeleton was clear, and the pseudopod was obvious. A CCK-8 assay was used to measure cell viability at different time points in Figure 4C. Our results indicated that the cell viability in the four groups of scaffolds was almost similar to that in the control group at 1 and 3 days. However, at 5 and 7 days, the cell viability of the SF-CS-GO group was higher than that of the SF and the SF-CS groups, while the cells exhibited a significantly higher proliferation in the SF-CS-GO-P24 group. These results showed that GO had a good biocompatibility and could promote cell adhesion and proliferation. This might be because GO roughens the surface of the scaffold, making it easier for cells to adhere. Moreover, its abundant functional groups could interact with cells and promote cell viability.⁵⁰ In addition, the modification of GO by P24 polypeptide could further improve the biocompatibility of the scaffolds, provide

more cell recognition sites, and promote cell adhesion and proliferation.⁵¹ These results showed that the four groups of scaffolds had a good biocompatibility and no cytotoxicity.

Polypeptide loading and active release of P24

The loading efficiency of P24 on GO-P24 and SF-CS-GO-P24 was respectively investigated by TGA analysis. Meanwhile, the release profile of P24 from SF-CS-GO-P24 scaffolds was also examined for a duration of 21 days. According to the TGA results in Figure 5A, the curve of GO showed a small loss of 10% weight in the range of 50°C–100°C, which was primarily attributed to the volatilization of water in π -stacked structure, and a strong loss of up to 73% weight in the 100°C–800°C range, which was primarily because of the decomposition of oxygen-containing groups in GO. The curve of GO-P24 showed a similar thermal degradation trend to GO but less residue, which indicated that the P24 content in the GO-P24 was ~13%. Compared to TGA curve of SF, SF-CS-GO-P24 curve in Figure 5B demonstrated a less loss of weight about 25%, which was equivalent to the GO containing in the SF-CS-GO-P24 scaffold. Based on these data, we could predict that the P24 loading on the SF-CS-GO-P24 scaffold was ~3.3%. In addition, the release curve of P24 from SF-CS-GO-P24 scaffolds is depicted in Figure 5C. P24 had a rapid release during the first 3 days, which we speculated due to the physical adsorption of P24 on the scaffold. Subsequently, the P24 was released in a slow and sustained manner. Until the 21st day, the P24 released was ~ (49.43%±2.93%). This result implied that GO-P24 was more suitable to help P24 continuously and steadily act with the cells adhered on the scaffolds as well as avoid the local rapid diffusion of P24. In order to further verify the activity of P24 grafted on SF-CS-GO and SF-CS-GO-P24 scaffolds, the ALP activity of cells cultured on the scaffolds was measured. As shown in Figure 5D, the cells seeded on the well plate and cultured with normal medium were used as the negative control, while cells cultured with the medium containing equivalent P24 to the SF-CS-GO-P24 scaffold were used as the positive control. Compared with negative control and SF-CS-GO, the ALP activity was higher in P24 positive control and SF-CS-GO-P24 scaffolds, indicating the effectiveness of P24 in promoting osteogenesis. However, cells growing on SF-CS-GO-P24 scaffolds showed a higher ALP activity than those cultured by pure P24, suggesting that grafting of P24 with GO did not change its bioactivity and SF-CS-GO-P24 scaffolds provided a more effective

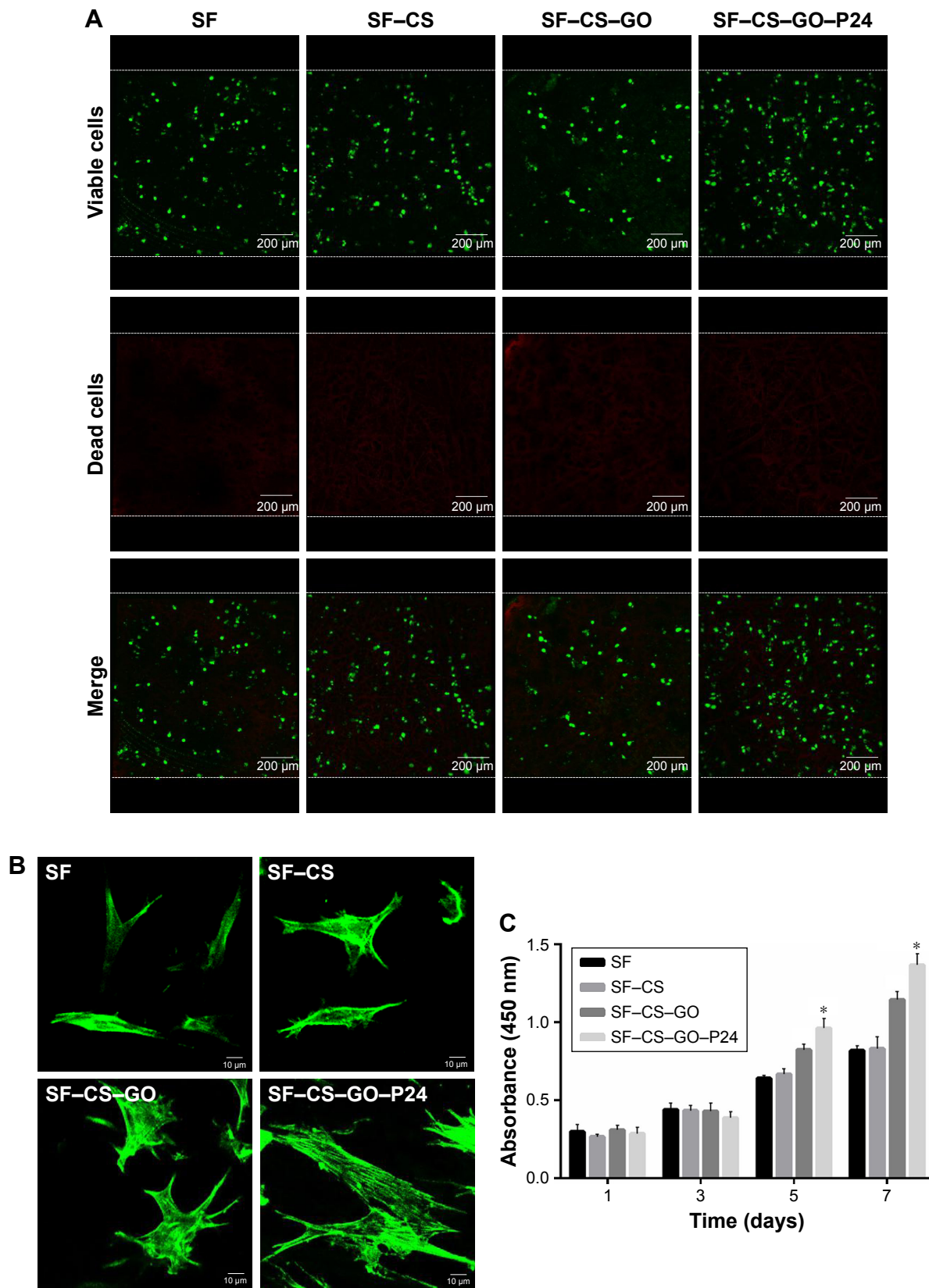


Figure 4 Biocompatibility of scaffolds.

Notes: (A) Live/dead assay was used to test the cytotoxicity of the scaffolds, with living cells staining as green by Calcein-AM and dead cells staining as red by PI (scale bars=200 μm). (B) The adherence shape of BMSCs cultured on different scaffolds were observed by a confocal microscope after 24 hours (scale bars=10 μm). (C) Assessing the proliferation of BMSCs seeded onto the scaffolds after 1, 3, 5 and 7 days by CCK-8 assay (n=3, *P<0.05 as compared with other groups of scaffolds).

Abbreviations: BMSC, bone marrow mesenchymal stem cell; Calcein-AM, Calcein-acetoxymethyl; CCK-8, cell counting kit-8; SF, silk fibroin; CS, chitosan; GO, graphene oxide.

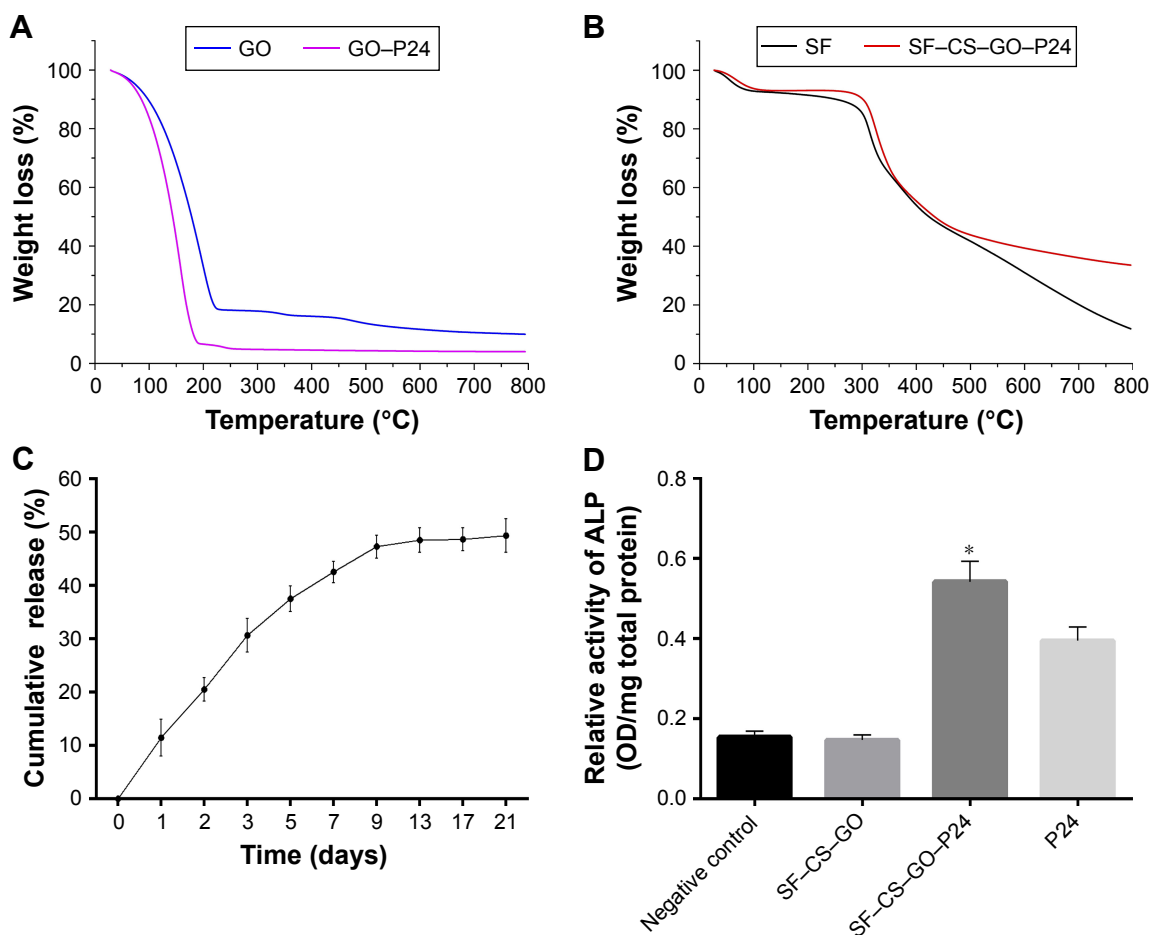


Figure 5 (A) TGA curves of GO and GO-P24. (B) TGA curves of SF and SF-GO-P24. (C) The cumulative release curve of P24 polypeptide from GO-P24 at 37°C in PBS. (D) ALP activity of BMSCs after 7 days of culture (n=3, *P<0.05 as compared with negative control, P24 positive control, and SF-CS-GO scaffolds).

Abbreviations: TGA, thermogravimetric analysis; GO, graphene oxide; SF, silk fibroin; BMSC, bone marrow mesenchymal stem cell; CS, chitosan.

matrix for cell differentiation and osteogenesis. This result was consistent with the previous study that showed that immobilizing P24 on matrix helped protect its activity and allowed it to play a long-term effect in a localized area.³⁷

Osteogenic differentiation of BMSCs on the composite scaffolds

The osteogenic differentiation of BMSCs is crucial for the repair of bone tissue defect.⁵² The effect of osteogenic differentiation of BMSCs seeded onto the different groups of scaffolds under osteogenic medium or normal conditions was evaluated by immunofluorescent staining and RT-PCR. First, the analysis in Figure 6 shows that when the cells were cultured under osteogenic medium conditions, the fluorescence intensity of osteogenic markers (OPN and COL I) was increased obviously in the SF-GO-CS-P24 group, followed by the SF-CS-GO group, while the SF and CS groups were the lowest and had no significant difference between them. However, the expressions of the OPN and

COL I in the SF-CS-GO-P24 group were upregulated, and there was no change in the other three groups when the cells were cultured under non-osteogenic medium conditions. The abovementioned results demonstrate that GO could increase the osteogenic differentiation of stem cells, whereas it needed other osteogenic differentiation factors to have synergistic effects, and the functionalization of GO with P24 made it more effective in promoting bone differentiation. As shown in Figure 7 of the RT-PCR analysis at different points of time, the Runx2 and ALP, as early markers of osteogenesis, had the highest relative expression level on the 7th day and decreased gradually on the 14th day, while the OPN and COL I were the late markers of osteogenesis, and the relative expression level was a continuous increase. The results demonstrated that SF-CS-GO and SF-CS-GO-P24 had higher ability to upregulate the expression of osteogenic-related genes in BMSCs under osteogenic medium condition. A large number of studies reported that GO could increase osteogenic differentiation of stem cells due to π - π stacking,

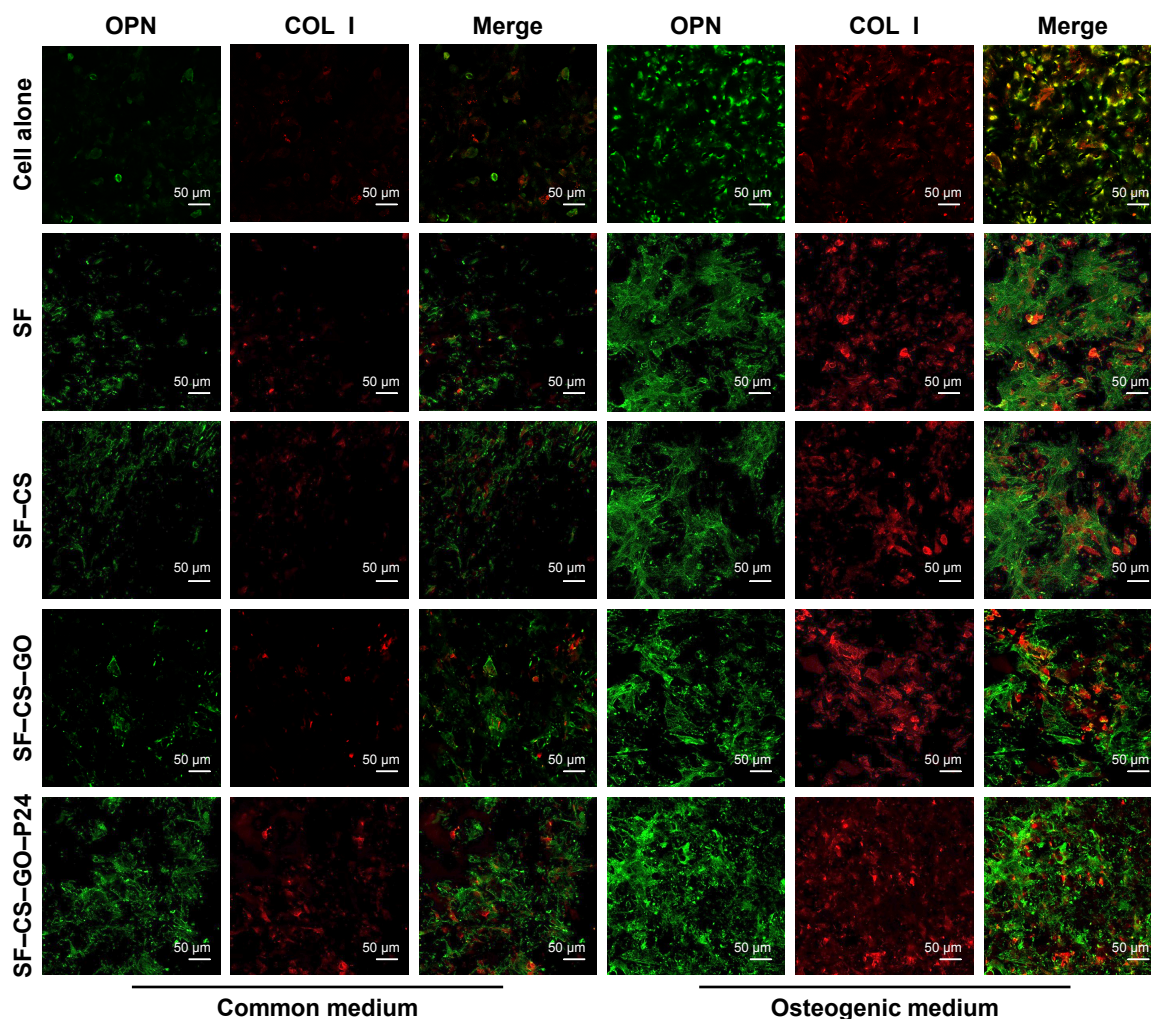


Figure 6 Immunofluorescence staining for OPN and COL I of BMSCs cultured on the scaffolds under common medium and osteogenic medium conditions (scale bars=50 µm). **Abbreviations:** BMSC, bone marrow mesenchymal stem cell; SF, silk fibroin; CS, chitosan; GO, graphene oxide.

electrostatic, and hydrophobic interaction with proteins,²⁷ while the surface of P24 contains phosphoserine, which also had affinity for calcium phosphate, eg, hydroxyapatite, and could regulate the structure and molecular conformation of nano-hydroxyapatite.⁵¹ Our experimental results reconfirmed some previous research results. The GO added to nanofiber scaffolds not only promoted the adhesion and proliferation of stem cells but also induced the osteogenic differentiation of stem cells into osteoblasts, which was of great significance for biomedical applications requiring the bionic extracellular matrix.

In vivo bone repair of calvarial defects

To further test the effects of composite scaffolds on bone defect repair, we implanted the material into the skull defects of rats. The skull specimens were harvested 8 weeks later, and the bone regeneration in the defects was analyzed by

micro-CT as shown in Figure 8A and B. As expected, the critical-sized bone defects could not heal by themselves, and there was no new bone formation in the no treatment group. There was only a little new bone formation in the SF and SF-CS groups on the edge of the defect, suggesting that the silk protein itself does not have osteogenic induction properties and is not suitable for bone defect repair alone. The SF-CS-GO group had better bone healing than SF, SF-CS, or control groups, while the SF-CS-GO-P24 group showed best bone repair and regeneration of the defects. As shown in Figure 8C, analysis of the bone mineral density in the defect areas demonstrated significantly higher values in the SF-CS-GO-P24 group than that in the other groups, exhibiting robust osteogenic activity. Histological analysis of bone regeneration was further performed by H&E and Masson trichrome staining in Figure 8D. There was seldom new bone tissue in the blank group, but the fibrous tissue filled the defect.

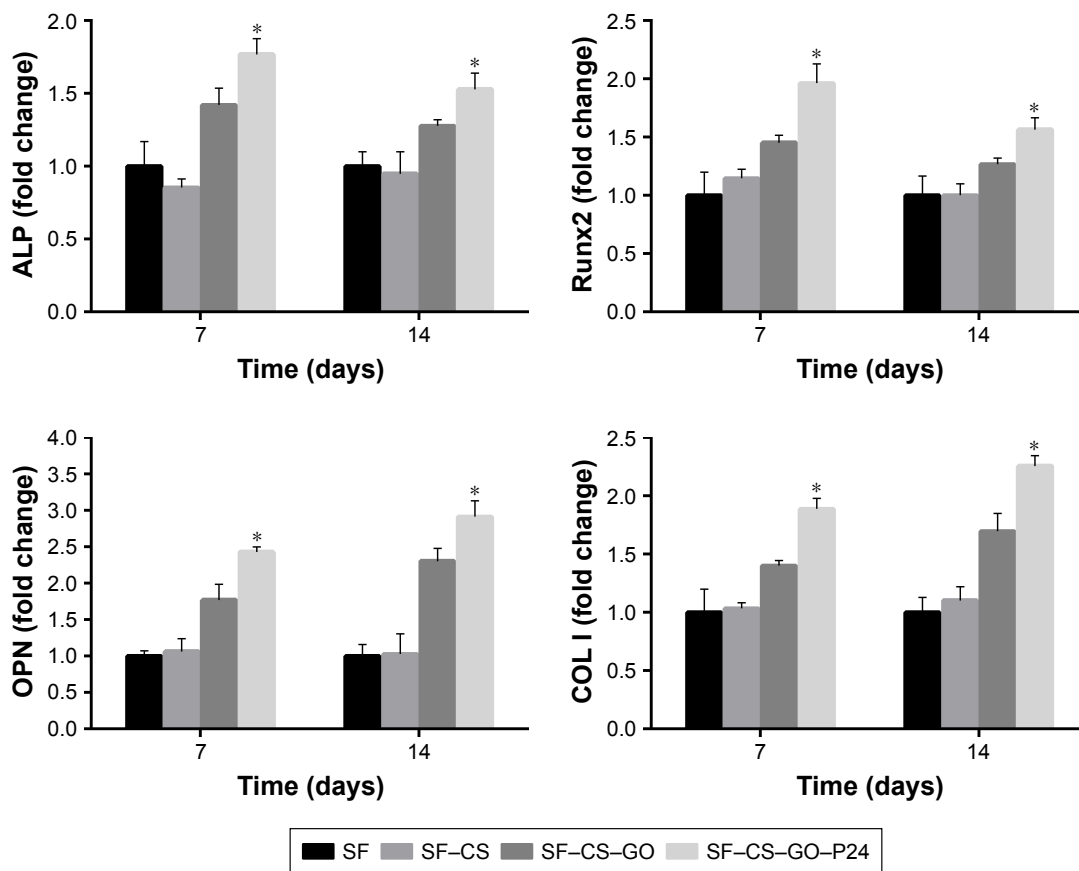


Figure 7 RT-PCR assay to test the expression of osteogenic-related genes (ALP, Runx2, OPN, and COL I) of BMSCs cultured on the scaffolds under osteogenic medium condition (n=3, *P<0.05 as compared with other groups of scaffolds).

Abbreviations: RT, real time; BMSC, bone marrow mesenchymal stem cell; SF, silk fibroin; CS, chitosan; GO, graphene oxide.

In SF and SF-CS groups, only part of new bone regeneration was found at the edge of the defect, while in the SF-CS-GO group, some new bone was found at the defect site due to the osteogenic effect of GO. In the SF-CS-GO-P24 group, the defects were almost filled with new bones; the native and new bone tissues fused with each other naturally. In general, according to *in vivo* data here, electrospun SF scaffolds coated with BMP-2-grafted GO have the potential to be a functional scaffold for the engineering of bone tissue. Actually, in order to further research on the SF-CS-GO-P24 scaffold and its application in bone regeneration, more analysis *in vivo* such as bone formation rate virtualized by fluorescent sequence labeling or vessel formation evaluation by micro-CT could be carried out in future study.

SF is a famous natural biomaterial that has been used for many years because of its excellent biocompatibility.⁹ The application of GO in tissue engineering has also been extensively studied. P24 polypeptide originating from the knuckle epitope of BMP-2 could be loaded into GO and further grafted onto the SF-based scaffold. In this study, as

shown in Figure 9, we grafted P24 onto GO by a chemical method and combined GO-P24 with SF electrospun scaffolds by electrostatic interaction between the positive charge of CS and the negative charge of GO-P24. The biocompatibility of the composite scaffolds and cell-specific osteogenic differentiation were further improved due to the modification of GO-P24. Meanwhile, more bone tissue repair and regeneration were achieved due to the biological activity of P24, which further illustrated the excellent osteogenic ability of the composite SF-CS-GO-P24 scaffolds. At present, GO-P24 showed advantages in cell spreading, proliferation, differentiation, and bone formation, which was mainly contributed by the characteristics of GO and P24, respectively. On the one hand, GO roughened the surface of the scaffold, making it easier for cells to adhere. Moreover, cell viability and osteogenic differentiation of BMSCs could also be promoted through the interaction between cells and the abundant functional groups on molecular structure of GO.^{28,50} On the other hand, P24 polypeptide can provide more cell recognition sites to promote cell adhesion and proliferation,⁵¹ when used for the

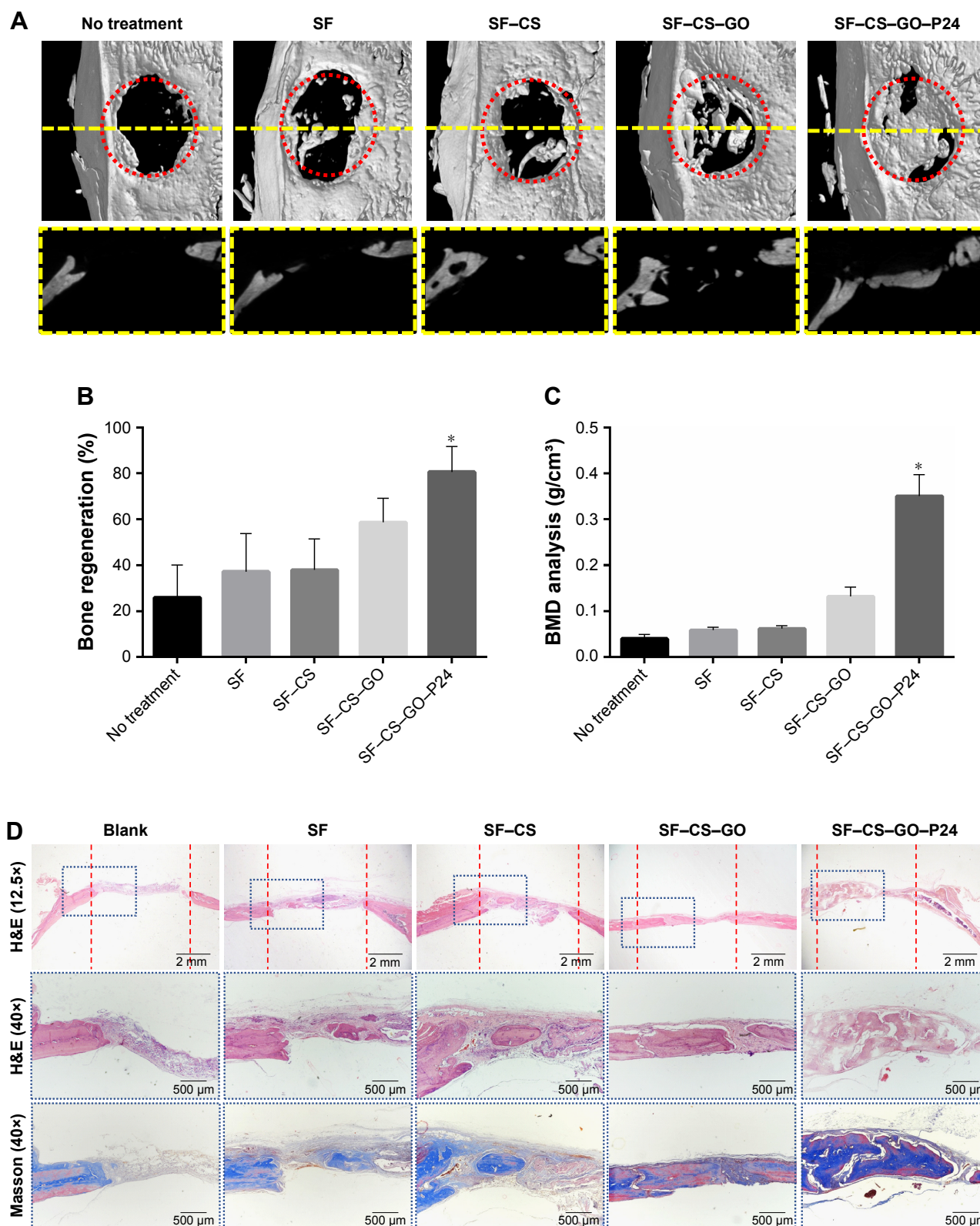


Figure 8 Micro-CT analysis of bone formation after the scaffold implantation into critical-sized bone defects 8 weeks later.

Notes: (A) Micro-CT images of the bone regeneration from the different groups of the scaffolds. The yellow dotted line shows bone regeneration in bone defect in the sagittal plane. (B and C) Quantification of the bone formation from the micro-CT images ($n=5$, $*P<0.05$ as compared with other groups of scaffolds). (D) Histological analysis using H&E and Masson trichrome staining. The red dotted line represents the defect area (scale bar=2 mm), and the blue dotted line is one side of the defect under a high magnification view (40x; scale bar=500 μm).

Abbreviations: CT, computed tomography; SF, silk fibroin; CS, chitosan; GO, graphene oxide.

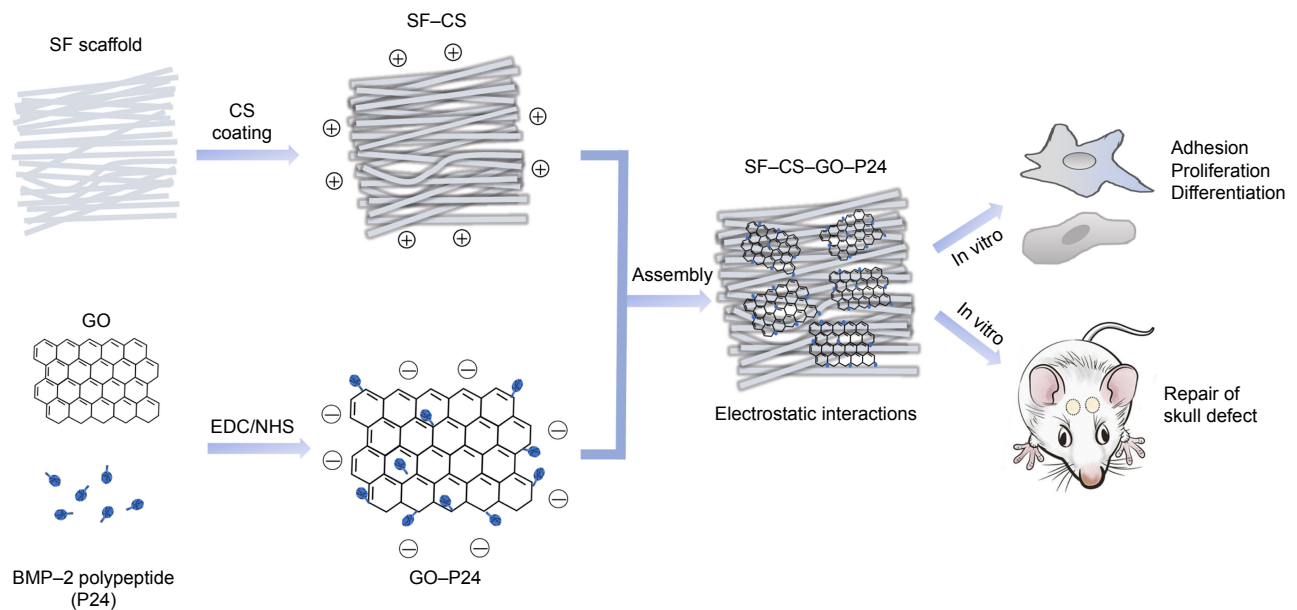


Figure 9 A brief schematic drawing of the design of this study.

Abbreviations: SF, silk fibroin; CS, chitosan; GO, graphene oxide; EDC, 1-(3-dimethylaminopropyl)-3-ethylcarbodiimide hydrochloride; NHS, N-hydroxysuccinimide.

surface functionalization of the composite scaffold. Since P24 polypeptide is a kind of BMP-2-derived peptide, it had been proved to be capable of enhancing the osteoblastic differentiation of BMSCs and inducing ectopic bone formation in a similar way to BMP-2.³⁷

Conclusion

In the present study, a BMP-2 polypeptide named P24 onto GO was successfully grafted, and the functionalized GO was used to cover a SF electrospun scaffold through electrostatic interactions. The composite scaffold showed a good biocompatibility, and the hydrophilicity, cell adhesion, and proliferation effects of the coated scaffolds improved compared to those of uncoated scaffolds. After immobilization of the GO-P24, the scaffold showed excellent biological activity, improving bone regeneration in critical-sized bone defects and enhancing the osteogenic differentiation of BMSCs. Taken together, we have innovatively modified GO and combined it with silk electrospun scaffolds for potential applications in tissue engineering and other biomedical fields.

Acknowledgments

This study was supported by the National Natural Science Foundation of China (81620108006, 31500787, 81430012, 51703127, 81801006, 31600777), the National Key Research and Development Program of China (2016YFC1102900), Young Elite Scientist Sponsorship Program by CAST (2017QNRC001), Shanghai Sailing Program (16YF1406600)

and Interdisciplinary Program of Shanghai Jiao Tong University (YG2015ZD06).

Disclosure

The authors report no conflicts of interest in this work.

References

- Hutmacher DW. Scaffolds in tissue engineering bone and cartilage. *Biomaterials*. 2000;21(24):2529–2543.
- Liu X, Ma PX, Px M. Polymeric scaffolds for bone tissue engineering. *Ann Biomed Eng*. 2004;32(3):477–486.
- Pina S, Oliveira JM, Reis RL. Natural-based nanocomposites for bone tissue engineering and regenerative medicine: a review. *Adv Mater*. 2015; 27(7):1143–1169.
- Gomes ME, Godinho JS, Tchalamov D, Cunha AM, Reis RL. Alternative tissue engineering scaffolds based on starch: processing methodologies, morphology, degradation and mechanical properties. *Mater Sci Eng C*. 2002;20(1–2):19–26.
- Agrawal CM, Ray RB. Biodegradable polymeric scaffolds for musculoskeletal tissue engineering. *J Biomed Mater Res*. 2001;55(2):141–150.
- Tibbitt MW, Anseth KS. Hydrogels as extracellular matrix mimics for 3D cell culture. *Biotechnol Bioeng*. 2009;103(4):655–663.
- Bhardwaj N, Kundu SC. Electrospinning: a fascinating fiber fabrication technique. *Biotechnol Adv*. 2010;28(3):325–347.
- Nisbet DR, Forsythe JS, Shen W, Finkelstein DI, Horne MK. Review paper: a review of the cellular response on electrospun nanofibers for tissue engineering. *J Biomater Appl*. 2009;24(1):7–29.
- Kaplan DL. Fibrous proteins-silk as a model system. *Polym Degrad Stab*. 1998;59(1–3):25–32.
- Vepari C, Kaplan DL. Silk as a biomaterial. *Prog Polym Sci*. 2007; 32(8–9):991–1007.
- Zhang X, Reagan MR, Kaplan DL. Electrospun silk biomaterial scaffolds for regenerative medicine. *Adv Drug Deliv Rev*. 2009;61(12):988–1006.
- Bhattacharjee P, Kundu B, Naskar D, et al. Silk scaffolds in bone tissue engineering: An overview. *Acta Biomater*. 2017;63:1–17.

13. Bhattacharjee P, Naskar D, Maiti TK, Bhattacharya D, Kundu SC. Non-mulberry silk fibroin grafted poly (ϵ -caprolactone)/nano hydroxyapatite nanofibrous scaffold for dual growth factor delivery to promote bone regeneration. *J Colloid Interface Sci.* 2016;472:16–33.
14. Shen X, Zhang Y, Gu Y, et al. Sequential and sustained release of SDF-1 and BMP-2 from silk fibroin-nanohydroxyapatite scaffold for the enhancement of bone regeneration. *Biomaterials.* 2016;106:205–216.
15. Burg KJ, Porter S, Kellam JF. Biomaterial developments for bone tissue engineering. *Biomaterials.* 2000;21(23):2347–2359.
16. Berger J, Reist M, Mayer JM, Felt O, Peppas NA, Gurny R. Structure and interactions in covalently and ionically crosslinked chitosan hydrogels for biomedical applications. *Eur J Pharm Biopharm.* 2004;57(1):19–34.
17. Willcox JAL, Kim HJ. A Molecular dynamics study of water flow across multiple layers of pristine, oxidized, and mixed regions of graphene oxide: effect of graphene oxide layer-to-layer distance. *ACS Nano.* 2017;11(2): pp 2187–pp 2193.
18. Georgakilas V, Tiwari JN, Kemp KC, et al. Noncovalent functionalization of graphene and graphene oxide for energy materials, biosensing, catalytic, and biomedical applications. *Chem Rev.* 2016;116(9): 5464–5519.
19. Dreyer DR, Park S, Bielawski CW, Ruoff RS. The chemistry of graphene oxide. *Chem Soc Rev.* 2010;39(1):228–240.
20. Zhu Y, Murali S, Cai W. Graphene and graphene oxide: synthesis, properties, and applications. *Cheminform.* 2010;22(46):5226.
21. Seabra AB, Paula AJ, de Lima R, Alves OL, Durán N. Nanotoxicity of graphene and graphene oxide. *Chem Res Toxicol.* 2014;27(2):159–168.
22. Yang X, Wang Y, Huang X, et al. Multi-functionalized graphene oxide based anticancer drug-carrier with dual-targeting function and pH-sensitivity. *J Mater Chem.* 2011;21(10):3448–3454.
23. Choi HY, Lee TJ, Yang GM, et al. Efficient mRNA delivery with graphene oxide-polyethylenimine for generation of footprint-free human induced pluripotent stem cells. *J Control Release.* 2016;235:222–235.
24. Allen BL, Kotchey GP, Chen Y, et al. Mechanistic investigations of horseradish peroxidase-catalyzed degradation of single-walled carbon nanotubes. *J Am Chem Soc.* 2009;131(47):17194–17205.
25. Kurapati R, Russier J, Squillaci MA, et al. Dispersibility-dependent biodegradation of graphene oxide by myeloperoxidase. *Small.* 2015;11(32): 3985–3994.
26. Yang K, Wan J, Zhang S, Zhang Y, Lee ST, Liu Z. In vivo pharmacokinetics, long-term biodistribution, and toxicology of PEGylated graphene in mice. *ACS Nano.* 2011;5(1):516–522.
27. Yang B, Wang Y, Xiao L, Hu X, Zhou G. Enhanced antibacterial effect of polypyrazole-graphene oxide composite. *Macromol Res.* 2017;25(1): 21–26.
28. Han L, Sun H, Tang P. Mussel-inspired graphene oxide nanosheet-enwrapped Ti scaffolds with drug-encapsulated gelatin microspheres for bone regeneration. *Biomater Sci.* 2018;5(1):1–8.
29. Chen D, Zhao M, Mundy GR. Bone morphogenetic proteins. *Growth Factors.* 2004;22(4):233–241.
30. Cao X, Chen D. The BMP signaling and in vivo bone formation. *Gene.* 2005;357(1):1–8.
31. Rawadi G, Vayssi re B, Dunn F, Baron R, Roman-Roman S. BMP-2 controls alkaline phosphatase expression and osteoblast mineralization by a Wnt autocrine loop. *J Bone Miner Res.* 2010;18(10):1842–1853.
32. Ruppert R, Hoffmann E, Sebald W. Human bone morphogenetic protein 2 contains a heparin-binding site which modifies its biological activity. *FEBS J.* 2010;237(1):295–302.
33. Vallejo LF, Brokelmann M, Marten S, et al. Renaturation and purification of bone morphogenetic protein-2 produced as inclusion bodies in high-cell-density cultures of recombinant *Escherichia coli*. *J Biotechnol.* 2002;94(2):185–194.
34. Poynton AR, Lane JM. Safety profile for the clinical use of bone morphogenetic proteins in the spine. *Spine.* 2002;27(16 Suppl 1): S40–S48.
35. Zara JN, Siu RK, Zhang X, et al. High doses of bone morphogenetic protein 2 induce structurally abnormal bone and inflammation in vivo. *Tissue Eng Part A.* 2011;17(9–10):1389–1399.
36. Haidar ZS, Hamdy RC, Tabrizian M. Delivery of recombinant bone morphogenetic proteins for bone regeneration and repair. Part A: Current challenges in BMP delivery. *Biotechnol Lett.* 2009;31(12):1817–1824.
37. Saito A, Suzuki Y, Ogata Si, Ohtsuki C, Tanihara M. Activation of osteo-progenitor cells by a novel synthetic peptide derived from the bone morphogenetic protein-2 knuckle epitope. *Biochim Biophys Acta.* 2003;1651(1–2):60–67.
38. He X, Ma J, Jabbari E. Effect of grafting RGD and BMP-2 protein-derived peptides to a hydrogel substrate on osteogenic differentiation of marrow stromal cells. *Langmuir.* 2008;24(21):12508–12516.
39. Zhou X, Feng W, Qiu K, et al. BMP-2 Derived Peptide and Dexamethasone Incorporated Mesoporous Silica Nanoparticles for Enhanced Osteogenic Differentiation of Bone Mesenchymal Stem Cells. *ACS Appl Mater Interfaces.* 2015;7(29):15777–15789.
40. Bilem I, Chevallier P, Plawinski L, Sone ED, Durrieu MC, Laroche G. RGD and BMP-2 mimetic peptide crosstalk enhances osteogenic commitment of human bone marrow stem cells. *Acta Biomater.* 2016;36: 132–142.
41. Chevalier MT, Gonzalez JS, Alvarez VA. Polymers for Peptide/Protein Drug Delivery. In: Thakur VK, Thakur MK, editors. *Handbook of Polymers for Pharmaceutical Technologies: Structure and Chemistry, Volume 1.* Hoboken: John Wiley & Sons, Inc.; 2015:433–456.
42. Marciano DC, Kosynkin DV, Berlin JM, et al. Improved synthesis of graphene oxide. *ACS Nano.* 2010;4(8):4806–4814.
43. Luo Y, Shen H, Fang Y, et al. Enhanced proliferation and osteogenic differentiation of mesenchymal stem cells on graphene oxide-incorporated electrospun poly(lactic-co-glycolic acid) nanofibrous mats. *ACS Appl Mater Interfaces.* 2015;7(11):6331–6339.
44. Fu C, Yang X, Tan S, Song L. Enhancing cell proliferation and osteogenic differentiation of mc3t3-e1 pre-osteoblasts by bmp-2 delivery in graphene oxide-incorporated PLGA/HA biodegradable microcarriers. *Sci Rep.* 2017;7(1):12549.
45. Hao Z, Song Z, Huang J, et al. The scaffold microenvironment for stem cell based bone tissue engineering. *Biomater Sci.* 2017;5(8):1382–1392.
46. Go DP, Gras SL, Mitra D, et al. Multilayered microspheres for the controlled release of growth factors in tissue engineering. *Biomacromolecules.* 2011;12(5):1494.
47. Chronakis IS. Novel nanocomposites and nanoceramics based on polymer nanofibers using electrospinning process-A review. *J Mater Process Technol.* 2005;167(2–3):283–293.
48. Wang L, Lu C, Zhang B, Zhao B, Wu F, Guan S. Fabrication and characterization of flexible silk fibroin films reinforced with graphene oxide for biomedical applications. *RSC Adv.* 2014;4(76):40312–40320.
49. You R, Xu Y, Liu G, Liu Y, Li X, Li M. Regulating the degradation rate of silk fibroin films through changing the genipin crosslinking degree. *Polym Degrad Stab.* 2014;109(3):226–232.
50. Ruiz ON, Fernando KA, Wang B, et al. Graphene oxide: a nonspecific enhancer of cellular growth. *ACS Nano.* 2011;5(10):8100–8107.
51. Wu B, Zheng Q, Guo X, Wu Y, Wang Y, Cui F. Preparation and ectopic osteogenesis in vivo of scaffold based on mineralized recombinant human-like collagen loaded with synthetic BMP-2-derived peptide. *Biomed Mater.* 2008;3(4):44111.
52. Derubeis AR, Cancedda R. Bone marrow stromal cells (BMSCs) in bone engineering: limitations and recent advances. *Ann Biomed Eng.* 2004;32(1):160–165.

International Journal of Nanomedicine**Dovepress****Publish your work in this journal**

The International Journal of Nanomedicine is an international, peer-reviewed journal focusing on the application of nanotechnology in diagnostics, therapeutics, and drug delivery systems throughout the biomedical field. This journal is indexed on PubMed Central, MedLine, CAS, SciSearch®, Current Contents®/Clinical Medicine,

Journal Citation Reports/Science Edition, EMBase, Scopus and the Elsevier Bibliographic databases. The manuscript management system is completely online and includes a very quick and fair peer-review system, which is all easy to use. Visit <http://www.dovepress.com/testimonials.php> to read real quotes from published authors.

Submit your manuscript here: <http://www.dovepress.com/international-journal-of-nanomedicine-journal>